Радиофизика и радиоастрономия, 2000, т. 5, №2, стр. 171-181

Mathematical Model of Spatial-Harmonic Magnetron with Cold Secondary-Emission Cathode

K. Schünemann[1], S. V. Sosnytskiy[2], and D. M. Vavriv[2]

[1]*Technical University Hamburg-Harburg, Arbeitsbereich Hochfrequenztechnik, D-21071 Hamburg, Germany*

[2]*Institute of Radio Astronomy, NAS of Ukraine, 4, Chervonopraporna St., 310002, Kharkov, Ukraine*
E-mail: vavriv@rian.kharkov.ua

Received by editor August, 6, 1999, rewritten November, 23, 1999

A self-consistent mathematical model of the spatial-harmonic magnetron with cold secondary-emission cathode is proposed for investigating both transient and steady-state processes. Characteristic features of the simulation of space charge effects, secondary-emission, and nonlinear electron-wave interaction are described. Illustrative examples of simulations are given in order to show peculiarities of the operation of the spatial-harmonic magnetron as compared to conventional magnetrons. Multi-stable states of the magnetron are described and the mechanism of their formation is proposed.

I. Introduction

Since the fifties, it has become clear that conventional magnetrons [1] do not operate effectively in the millimeter-wave band because of three main limitations, which are inherent in their design. At first, the dimensions of the magnetron cavity become too small since they scale as λ, the wavelength. At second, the dc magnetic field grows as $1/\lambda$. At third, the necessary current density and back-bombarding are so intense that the life-time of thermionic cathodes is too short from the point of view of practical applications. Several solutions have been proposed to overcome these problems and to develop the effective tubes for millimeter-wave band. Spatial-harmonic magnetrons with secondary-emission cathode (SHM) can be considered as the most successful alternative to conventional magnetrons [2]. These magnetrons utilize first backward space harmonic of the $\pi/2$ or neighboring mode as working mode. That allows to increase the magnetron cavity dimensions by several times, and to decrease the needed values of dc magnetic field by a factor of about four. The problem of the cathode lifetime has been successfully solved by introducing a cold secondary-emission cathode rather than thermionic one. At present, SHMs are available for frequencies as high as 140 GHz where they can provide 10 kW peak output power [3]. These magnetrons offer also low-voltage, compact, and lightweight advantages and are now coming into use in various practical systems [4,5].

For a long time, the development and modifications of the SHM have been based on empirical rules accumulated from a large volume of experimental data. However, at present a demand has arisen for a nonlinear self-consistent analysis of such magnetrons that will allow to examine adequately the physics of their operation with the aim of a further enhancement of their performance. In this paper, a contribution has been made to the development of such a theory. We propose a mathematical model, which allows for all principal effects determining magnetron operation. We also present illustrative examples of simulations in order to show characteristic features of the SHM operation as compared to conventional magnetrons. The paper is organized as follows. In Section II, we describe the basic physical phenomena underlying the SHM operation. Section III deals with the equations of excitation of the magnetron cavity. The space charge description is given in Section IV. Section V contains the formulation of the equations of motion. The modelling of the secondary-emission is discussed in Section VI. The complete mathematical model is described in Section VII together with illustrative examples of some simulations. The Appendix contains the derivation of the norm of the magnetron cavity.

II. Physical model

There are three basic processes which determine the physics of SHM operation: 1) secondary-emission from a cold cathode initiated by a bombarding current, 2) space charge formation limiting secondary emission and affecting electron trajectories, and 3) the wave-particle interaction in the presence of dc, rf, and space charge fields. All these processes are interrelated to a great extent. Each of these processes has its peculiarities compared to classical magnetrons that should be taken into account when developing the corresponding mathematical model and methods for its study.

As for the secondary-emission, it usually takes place also in classical magnetrons with thermionic cathode. However, its contribution to the total current is not a principal one there. The electron bombarding of the cathode is mainly used for heating the thermionic cathode. The total current in the SHM, on the other hand, is only due to the secondary-emission from a cold cathode, which is typically made of a copper core coated with a platinum foil [1,2]. Therefore, the accurate modelling of the secondary-emission is of principal importance for any SHM simulation. This modelling so far can be based mainly on empirical results concerning secondary-emission properties of platinum or other materials which are used for coating the cold cathode. In particular, the dependence of the secondary-emission coefficient versus both impact energy and impact angle, and the directional diagram for the secondary electrons are needed for modelling.

The modelling of the space charge effects in the SHM also has its special features. Simulation and analysis of physical processes in classical magnetrons are usually based on the assumption of periodicity of the space charge known as the formation of spokes with an angle period of $2\pi/(n+mM)$, where n means mode number, m space harmonic number, and M number of anode resonators. It appeared (see Section VII) that this assumption is not valid for the magnetrons under investigation. It becomes clear that the simulation of such magnetrons is a more complicated task since the complete interaction space should be considered rather than the angle period of $2\pi/(n+mM)$ only.

The wave-particle interaction in the SHM is realized as an interaction of electrons with the first backward harmonic of the $\pi/2$-mode (or $(\pi/2-1)$-mode) in contrast to the classical magnetrons where the principal harmonic of the π-mode is used as the working mode. The backward harmonic is localized near the anode structure so that, in order to realize an effective electron-field interaction, the value of the dc magnetic field B should be chosen close to its critical value $B_{cr} \equiv r_a\sqrt{8m_0U_a/e_0}(r_a^2-r_c^2)^{-1}$. Here U_a means anode voltage, r_a and r_c anode and cathode radii, respectively, m_0 electron mass, and e_0 magnitude of electron charge. Typical positions of operating points for the SHM and for classical magnetrons are indicated in the parameter plane (dc magnetic field B) versus (anode voltage U_a) in Fig. 1. Curve a represents the dependence of the cut-off voltage vs. B. Curves b_1 and b_2 are Hartree's threshold voltages vs. B for the first backward harmonic of the $\pi/2$-mode and for the principal harmonic of the π-mode, respectively. The position of the operating point for the SHM is much closer to the cut-off parabola than that of the classical magnetron.

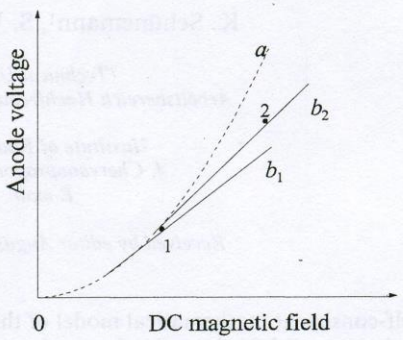

Fig. 1. *Parameter plane (dc magnetic field) versus (anode voltage) with the parabola of the cut-off voltage (dashed curve). Curves b_1 and b_2 are Hartree's threshold voltages vs. B for the first backward harmonic of the $\pi/2$-mode and for the principal harmonic of the π-mode, respectively. Points 1 and 2 indicate the typical location of the operation point for spatial-harmonic magnetrons and for classical magnetrons, respectively*

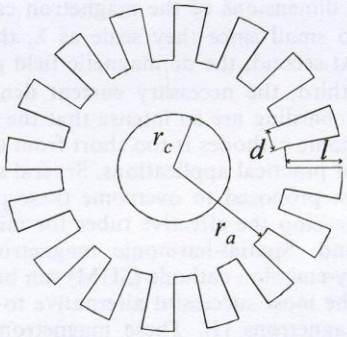

Fig. 2. *Geometry of the magnetron cavity*

When modelling the wave-particle interaction in the SHM as in the case of classical magnetrons, it can be assumed that the spatial field structure in the presence of electrons is the same as in the "cold" cavity. Thus, the mode field structure and the natural frequencies can be found from the solution of a boundary value problem. The geometry of the SHM oscillatory circuit, shown in Fig. 2, is usually the same as that for classical magnetrons, that allows using corresponding results on natural oscillations of the magnetron cavity. By now, approaches have been developed to determine the field structure, the natural frequency, and the mode Q-factor of the magnetron cavity with rather high accuracy [6,7]. An example of the cal-

culation of resonant mode frequencies of a loaded magnetron cavity together with values of the Q-factor is shown in Fig. 3. This figure illustrates a practical advantage of the used $\pi/2$-mode or neighboring ones as operating mode. The advantage is a better mode separation in comparison with the π-mode, as one can learn from the figure. It can be seen that the distance between neighboring modes on the frequency scale is drastically larger for the $\pi/2$-mode (n = 4) as compared to that for the π-mode (n = 8). These simulation results as well as experimental studies [1,2] allow to assume that modelling the SHM can be based on a single mode approximation, at least during the first stage of development of the theory.

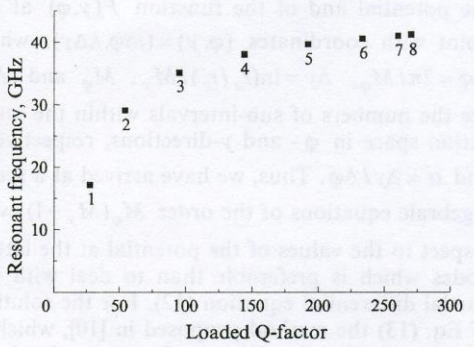

Fig. 3. *Resonant frequencies and Q-factors of the magnetron cavity modes with mode number 1 to 8*

When approximating the field structure, both synchronous and principal harmonics of the anode periodic structure must be taken into account rather than only a synchronous harmonic as in the case of classical magnetrons. This is due to the fact that the principal harmonic amplitude is much larger than the amplitude of the synchronous harmonic.

The SHM model proposed in this paper involves all the processes mentioned above, which are described in a two-dimensional frame assuming non-relativistic motion of the particles. The mathematical description of this model is given in the following sections. We start the derivation with a description of the cavity field.

III. Equations of Cavity Excitation

In the framework of the single mode approximation, the rf-electromagnetic field excited in the magnetron cavity can be written in a form

$$\vec{E}_{rf}(\vec{r},t)=\mathrm{Re}\left\{C_n(t)\vec{E}_n(\vec{r})e^{-i(\omega_n t+\psi)}\right\}. \qquad (1)$$

Here $C_n(t)$ means dimensionless field amplitude of the n-th mode, $\psi\equiv\psi(t)$ is the phase of the field, ω_n is a natural frequency of the mode, and $\vec{E}_n(\vec{r})$ is the spatial field distribution. In two-dimensional approximation, the radial and angular components of $\vec{E}_n(\vec{r})$ for the cavity shown in Fig. 2 are given by the expressions [8]:

$$E_{nr}=i\frac{EM}{\pi}\frac{1}{kr}\sum_{m=-\infty}^{+\infty}\sin(\gamma\theta)\frac{Z_\gamma(kr)}{Z'_\gamma(kr_a)}e^{-i\gamma\varphi}, \qquad (2)$$

$$E_{n\varphi}=\frac{EM}{\pi}\sum_{m=-\infty}^{+\infty}\frac{\sin\gamma\theta}{\gamma}\frac{Z'_\gamma(kr)}{Z'_\gamma(kr_a)}e^{-i\gamma\varphi}. \qquad (3)$$

Here r and φ are the polar coordinates, $\theta=d/2r_a$ is the normalized half-width of the anode slots, $k=\omega_n/c$ means the wave number with c being the light velocity, $Z_\gamma(kr)=J_\gamma(kr)-\frac{J'_\gamma(kr)}{J'_\gamma(kr_a)}N_\gamma(kr)$, where $J_\gamma(kr)$ and $N_\gamma(kr)$ are, respectively, Bessel and Neumann functions of the order $\gamma=n+mM$. E is a normalization coefficient having the dimensionality of the field strength. For the sake of convenience, this coefficient is chosen to be $E=2U_a/d$.

For practical tubes, the condition $\gamma>>kr_c$ usually holds that allows using the following asymptotic expressions for the spatial distribution of the field components instead of using Eqs. (2) and (3):

$$E_{nr}=i\frac{2U_aM}{\pi d}\frac{R_a}{R}\sum_{m=-\infty}^{+\infty}\frac{\sin\gamma\theta}{\gamma}\frac{R^\gamma+R^{-\gamma}}{R_a^\gamma-R_a^{-\gamma}}e^{-i\gamma\varphi}, \qquad (4)$$

$$E_{n\varphi}=\frac{2U_aM}{\pi d}\frac{R_a}{R}\sum_{m=-\infty}^{+\infty}\frac{\sin\gamma\theta}{\gamma}\frac{R^\gamma-R^{-\gamma}}{R_a^\gamma-R_a^{-\gamma}}e^{-i\gamma\varphi}, \qquad (5)$$

where $R=r/r_c$, $R_a=r_a/r_c$.

Amplitude $C_n(t)$ and phase $\psi\equiv\psi(t)$ of the cavity mode are governed by the equations of cavity excitation [9], which can be written as:

$$\frac{dC_n}{dt}=-C_n\frac{\omega_n}{2Q_n}-\mathrm{Re}\left\{\frac{1}{N_n}\left\langle\int_V\vec{j}(\vec{r},t)\vec{E}_n^*(\vec{r})e^{i\omega t}dV\right\rangle\right\}, \qquad (6)$$

$$\frac{d\psi}{dt} = \frac{1}{C_n}\mathrm{Im}\left\{\frac{1}{N_n}\left\langle \int_V \vec{j}(\vec{r},t)\vec{E}_n^*(\vec{r})e^{i\omega t}\,dV \right\rangle\right\}. \quad (7)$$

Here Q_n means the mode Q-factor, N_n is the mode norm which is calculated in the Appendix, $\vec{j}(\vec{r},t)$ is the current density in the interaction space, V is the cavity volume, and $\langle ... \rangle$ means averaging over the period of the rf oscillations.

Keeping in mind that the simulation of magnetron operation will be based on the representation of the electron cloud by a set of macroparticles, we rewrite the integral involved in Eqs. (6) and (7) as:

$$I \equiv \int_V \vec{j}(\vec{r},t)\vec{E}_n^*(\vec{r})e^{i(\omega_n t+\psi)}\,dV =$$

$$= q_0 \sum_{k=1}^{K_p} \left\{\dot{r}_k E_{nr}^*(r_k,\varphi_k) + r_k\dot{\varphi}_k E_{n\varphi}^*(r_k,\varphi_k)\right\} e^{i(\omega_n t+\psi)}, \quad (8)$$

where q_0 means charge of the macroparticle, K_p is the number of macroparticles used in the simulation, r_k and φ_r are polar coordinates of the k-th macroparticle, and the overdot means derivative with respect to time. The coordinates of each particle and their derivatives can be found from the equations of motion. In order to formulate these equations, an expression for the space charge field should first be specified.

IV. Space Charge Field

The calculation of the space charge field leads to the solution of Poisson's equation:

$$\frac{1}{r}\frac{\partial}{\partial r}\left(r\frac{\partial\Phi}{\partial r}\right) + \frac{1}{r^2}\frac{\partial^2\Phi}{\partial\varphi^2} = -\frac{\rho(r,\varphi)}{\varepsilon_0}, \quad (9)$$

where $\rho(r,\varphi)$ means the space charge density distribution and ε_0 is the permittivity of free space. In order to separate the space charge field potential from the potential introduced by the applied anode voltage, the following boundary conditions are used:

$$\Phi\big|_{r=r_c} = \Phi\big|_{r=r_a} = 0. \quad (10)$$

Poisson's equation can then be simplified by applying a coordinate transformation [10]:

$$r = r_c e^{y}. \quad (11)$$

In terms of this new coordinate, Eq. (9) reads:

$$\frac{\partial^2}{\partial y^2}\Phi + \frac{\partial^2}{\partial\varphi^2}\Phi = F(y,\varphi), \quad (12)$$

where $F(y,\varphi) = -\frac{r_c^2}{\varepsilon_0}e^{2y}\rho(y,\varphi)$.

For a numerical solution of Eq. (12), we rewrite it in a finite-difference form:

$$\alpha^2\left(\Phi_{i+1,k} - 2\Phi_{ik} + \Phi_{i-1,k}\right) +$$

$$+ \Phi_{i,k+1} - 2\Phi_{ik} + \Phi_{i,k-1} = (\Delta y)^2 F_{ik}, \quad (13)$$

$$i \in (0, M_\varphi - 1),\ k \in (1, M_y - 1).$$

Here Φ_{ik} and F_{ik} are, respectively, the values of the potential and of the function $F(y,\varphi)$ at the point with coordinates $(\varphi, y) = (i\Delta\varphi, k\Delta y)$, where $\Delta\varphi = 2\pi/M_\varphi$, $\Delta y = \ln(r_a/r_c)/M_y$, M_φ and M_y are the numbers of sub-intervals within the interaction space in φ- and y-directions, respectively, and $\alpha = \Delta y/\Delta\varphi$. Thus, we have arrived at a set of algebraic equations of the order $M_\varphi(M_y - 1)$ with respect to the values of the potential at the lattice nodes which is preferable than to deal with the partial differential equation (12). For the solution of Eq. (13) the method proposed in [10], which is based on the fast Fourier transformation, has been used.

Let us now consider in more detail a way of calculating the F_{ik}-values. As far as the space charge is represented with a set of macroparticles, its density can be written in a form:

$$\rho(y,\varphi) = \frac{q_0}{L}\sum_{j=1}^{K_{part.}} \delta(y - y_j)\delta(\varphi - \varphi_j), \quad (14)$$

where y_j, φ_j are coordinates of the j-th macroparticle and L means the axial length of the interaction space. The so-called "cloud-in-cell" method [11] is used in order to assign a charge value to each node of the lattice. According to this method, the charge of a particle with coordinates y_j, φ_j is shared between four neighboring nodes by using the rules:

$$q_{ik} = (1-a)(1-b)q_0, \qquad q_{i+1,k} = a(1-b)q_0,$$
$$q_{i,k+1} = (1-a)bq_0, \qquad q_{i+1,k+1} = abq_0, \quad (15)$$

where $a = (\varphi_j - \varphi_i)/\Delta\varphi$, $b = (y_j - y_i)/\Delta y$.

By using these rules, one arrives at the following expression for F_{ik}:

$$F_{ik} = -\frac{q_{ik}}{\varepsilon_0 \, L \, \Delta\varphi \, \Delta y}. \tag{16}$$

Provided that the solution of Eq. (13) has been found, the components of the space charge field strength are given by the expressions:

$$E_r^{ch} \equiv -\frac{\partial \Phi}{\partial r} = -\frac{e^{-y}}{r_c}\frac{\partial \Phi}{\partial y},$$

$$E_\varphi^{ch} \equiv -\frac{1}{r}\frac{\partial \Phi}{\partial \varphi} = -\frac{e^{-y}}{r_c}\frac{\partial \Phi}{\partial \varphi}, \tag{17}$$

where

$$\frac{\partial \Phi}{\partial y} = \frac{(1-a)}{\Delta y}\left(\Phi_{i,k+1} - \Phi_{ik}\right) + \frac{a}{\Delta y}\left(\Phi_{i+1,k+1} - \Phi_{i+1,k}\right),$$

$$\frac{\partial \Phi}{\partial \varphi} = \frac{(1-b)}{\Delta \varphi}\left(\Phi_{i+1,k} - \Phi_{ik}\right) + \frac{b}{\Delta \varphi}\left(\Phi_{i+1,k+1} - \Phi_{i,k+1}\right). \tag{18}$$

Here a and b mean the same as in Eq. (15).

Having expressions for the rf components of the cavity field (see Eqs. (4), (5)) and also for the components of the space charge field, we can proceed to the equations of motion.

V. The Equations of Motion

In polar coordinates, the equations of motion for an arbitrary electron in the interaction space can be written as

$$\begin{cases} \ddot{r} - r\dot{\varphi}^2 = \dfrac{e_0}{m_0}\left[\dfrac{U_a}{\ln(r_a/r_c)\, r} + \dfrac{\partial \Phi(r,\varphi,t)}{\partial r} - E_r^{rf}(r,\varphi,t) - Br\dot{\varphi}\right], \\ r\ddot{\varphi} + 2\dot{r}\dot{\varphi} = \dfrac{e_0}{m_0}\left[B\dot{r} - E_\varphi^{rf}(r,\varphi,t) - \dfrac{1}{r}\dfrac{\partial \Phi(r,\varphi,t)}{\partial \varphi}\right], \end{cases} \tag{19}$$

where the components of the rf-field are given by the expressions:

$$E_r^{rf} = C_n \operatorname{Re}\left\{E_{nr}(r,\varphi)\, e^{-i(\omega_n t + \psi)}\right\}$$

$$E_\varphi^{rf} = C_n \operatorname{Re}\left\{E_{n\varphi}(r,\varphi)\, e^{-i(\omega_n t + \psi)}\right\}, \tag{20}$$

with $E_{nr}(r,\varphi)$ and $E_{n\varphi}(r,\varphi)$ given by Eqs. (4), (5).

Now let us rewrite the equations of motion in terms of the variables y, φ and the dimensionless time $\tau = \Omega t$ with $\Omega = e_0 B / m_0$ being the cyclotron frequency:

$$\begin{cases} \ddot{y} + \dot{y}^2 - \dot{\varphi}^2 + \varphi = e^{-2y}\left[A + \dfrac{\partial \Phi'}{\partial y} - C_n \sum\limits_{m=-\infty}^{\infty} \varepsilon_m \left(e^{\gamma\theta} + e^{-\gamma\theta}\right) \sin\left(\gamma\varphi + \upsilon\tau + \psi\right)\right], \\ \ddot{\varphi} + 2\dot{y}\dot{\varphi} - \dot{y} = e^{-2y}\left[\dfrac{\partial \Phi'}{\partial \varphi} - C_n \sum\limits_{m=-\infty}^{\infty} \varepsilon_m \left(e^{\gamma\theta} - e^{-\gamma\theta}\right) \cos\left(\gamma\varphi + \upsilon\tau + \psi\right)\right]. \end{cases} \tag{21}$$

Here $A = \dfrac{e_0 U_a}{m_0 r_c^2 \Omega^2 \ln(r_a / r_c)}$ is a coefficient describing the effect of anode voltage on particle motion, $\varepsilon_m = \dfrac{e_0 U_a}{m_0 r_c^2 \Omega^2}\dfrac{M}{\pi}\dfrac{\sin\gamma\theta}{\gamma\theta}\dfrac{1}{R_a^{\gamma} - R_a^{-\gamma}}$ are coefficients describing relations between the spatial harmonics of the anode structure, $\upsilon = \omega_n / \Omega$ means the normalized natural frequency of the working mode, and $\Phi'(y,\varphi) = e_0 \Phi(y,\varphi)/(m_0 r_c^2 \Omega^2)$ is the normalized potential of the space charge field. These equations should be supplemented with initial conditions for both "thermal" electrons, which are produced by the auxiliary side cathode, and secondary-emission electrons from the cold cathode. In order to specify the initial conditions for the "thermal" electrons, the problem for the injection of these electrons should be solved. However, these electrons should be taken into account only in the initial stage of the field development. The analysis of the steady-state oscillations can be performed without considering the "thermal" electrons since their amount is negligibly small compared to the amount of the secondary-emission electrons. As for the initial conditions for the latter electrons, they should be specified at the cathode where y = 0. The initial values for other variables are defined by secondary-emission processes, which will be considered in the next section. The electron trajectories determined by Eq. (20) and by the initial conditions should be calculated until the variable y becomes zero or $\ln(r_a / r_c)$, what means that the particular electron has reached either the cathode or the anode surface, respectively. By impacting the cathode, an electron causes the secondary-emission.

VI. The Secondary-Emission

The description of secondary-emission is complicated by the lack of an adequate mathematical

model of this process. Usually, experimental data are used in order to establish relations between primary and secondary electrons. In this paper, the following assumptions are applied in accordance with [12,13]:

1) The secondary-emission electrons encompass "truly" secondary electrons and inelastically reflected ones. The energy of the former electrons is distributed between 0 and 50 eV with a maximum at 0 eV, the energy of the latter is located between 50 eV and the energy of a primary electron. The energy distribution of the inelastically reflected electrons is yet imperfectly understood. Therefore, it has been assumed to be a homogeneous one.

2) The "truly" secondary emission coefficient δ and the inelastic reflection coefficient η depend on the energy of the primary electron w_0 (impact energy). The coefficient δ also depends on the incidence angle α of the primary electron. The relation between δ and α is described according to

$$\delta(w_0,\alpha)=\delta_0\left(\frac{w_0}{1+\alpha^2/\pi}\right)\left[1+\alpha^2/(2\pi)\right]. \qquad (22)$$

Here $\delta_0(w_0)$ means the secondary-emission coefficient for normal incidence angle. The dependences of the secondary emission coefficient and the inelastic reflection coefficient versus impact energy for normal incidence angle have been approximated in the case of platinum by

$$\eta=0.47\left(1-e^{-2.3w_0}\right), \qquad (23)$$

$$\delta_0=\begin{cases}\sqrt{5w_0} & w_0<0.3,\\ 1.39-0.8(0.8-w_0)^2 & 0.3\le w_0\le 1,\\ 1.57e^{-0.14w_0} & w_0\ge 1.\end{cases} \qquad (24)$$

Here the impact energy w_0 is measured in keV. These approximations are shown in Fig. 4 together with corresponding experimental data published in [12]. The agreement is good.

3) Both "truly" secondary electrons and the inelastically reflected ones leave the cathode surface at randomly distributed angle β, which is the angle between the cathode normal vector and the electron velocity vector after leaving the cathode. The probability that this electron leaves the cathode at some angle β is proportional to $\cos\beta$.

Having specified the processes on the cold cathode, the equations of motion, the space charge field, and the equations of cavity excitation we can proceed to the formulation of the final mathematical model.

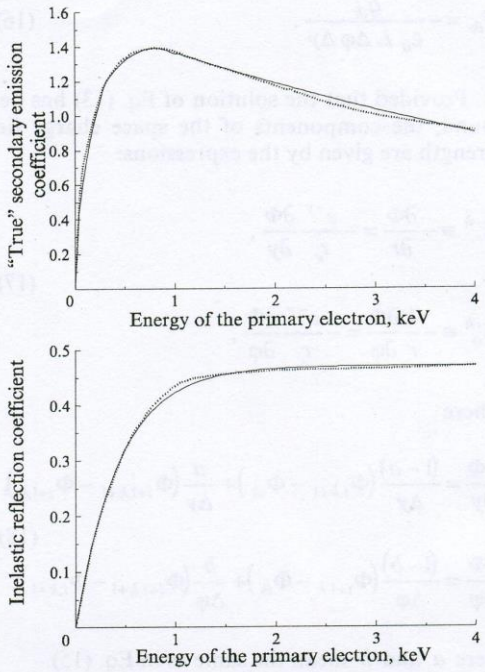

Fig. 4. *Dependence of the secondary-emission coefficient and the inelastic reflection coefficient on the energy of the primary electron:*
solid curve – approximation, dashed curve – experimental data

VII. Mathematical Model

Let us start from integral (8), which is proportional to the complex power of electron-wave interaction. With respect to the variables and dimensionless parameters involved in Eq. (21), this integral can be written as:

$$I=\frac{q_0}{e_0}m_0r_c^2\Omega^3\times$$
$$\times\sum_{j=1}^{k_p}\sum_{m=-\infty}^{\infty}\varepsilon_m\left[-i\dot{\gamma}_j\left(e^{\gamma\nu_j}+e^{-\gamma\nu_j}\right)+\dot{\varphi}_j\left(e^{\gamma\nu_j}+e^{-\gamma\nu_j}\right)\right]e^{i(\upsilon\tau+\psi+\gamma\varphi_j)}. \qquad (25)$$

Real and imaginary parts multiplied by C_n are equal to the active and reactive power of the interaction between the electrons and the rf-field in the magnetron, respectively. In terms of I, the equations of cavity excitation (6), (7) read:

$$\dot{C}_n = -C_n \frac{\omega_n}{2Q\Omega} - \frac{1}{N_n \Omega} \mathrm{Re}\langle I \rangle , \qquad (26)$$

$$\dot{\psi} = \frac{1}{N_n \Omega} \frac{1}{C_n} \mathrm{Im}\langle I \rangle .$$

Rewriting these equations in dimensionless parameters and supplementing them with the equations of motion and the expression for the space charge field, we arrive at the mathematical model of the magnetron:

$$\dot{C}_n = C_n \frac{\upsilon}{2} \left(S_1(C_n, \psi) - \frac{1}{Q_n} \right), \qquad (27)$$

$$\dot{\psi} = -\frac{\upsilon}{2} S_2(C_n, \psi), \qquad (28)$$

$$\ddot{y} + \dot{y}^2 - \dot{\varphi}^2 + \dot{\varphi} = e^{-2y} \times$$
$$\times \left[A + \frac{\partial \Phi'}{\partial y} - C_n \sum_{m=-\infty}^{\infty} \varepsilon_m \left(e^{\gamma y} + e^{-\gamma y} \right) \sin(\gamma\varphi + \upsilon\tau + \psi) \right], \qquad (29)$$

$$\ddot{\varphi} + 2\dot{y}\dot{\varphi} - \dot{y} =$$
$$= e^{-2y} \left[\frac{\partial \Phi'}{\partial \varphi} - C_n \sum_{m=-\infty}^{\infty} \varepsilon_m \left(e^{\gamma y} - e^{-\gamma y} \right) \cos(\gamma\varphi + \upsilon\tau + \psi) \right], \qquad (30)$$

$$\frac{\partial^2 \Phi'}{\partial y^2} + \frac{\partial^2 \Phi'}{\partial \varphi^2} = F'(y, \varphi). \qquad (31)$$

Here

$$\begin{pmatrix} S_1 \\ S_2 \end{pmatrix} = \begin{pmatrix} \mathrm{Re} \\ \mathrm{Im} \end{pmatrix} \frac{G}{C_n} \times$$
$$\times \left\langle \sum_{j=1}^{k_p} \sum_{m=-1}^{0} \varepsilon_m \left[-i\dot{y}_j \left(e^{\gamma y_j} + e^{-\gamma y_j} \right) + \dot{\varphi}_j \left(e^{\gamma y_j} + e^{-\gamma y_j} \right) \right] \times \right.$$
$$\left. \times e^{i(\upsilon\tau + \psi + \gamma\varphi_j)} \right\rangle, \qquad (32)$$

are the oscillatory characteristics of the magnetron describing the effect of the electrons on the development of the cavity mode, $F'(y,\varphi) = \dfrac{e_0}{m_0 r_c^2 \Omega^2} F(y,\varphi)$ is a function describing the space charge distribution in the interaction space at any moment of time, and $G = -2q_0 m_0 r_c^2 \Omega^3 / (e_0 N_n \omega_n)$ is a dimensionless parameter.

Solving this set of equations with corresponding initial conditions, one can find the evolution of the amplitude and the phase of the resonator field and the power characteristics, like the power extracted from a dc supply (P_0), the electron efficiency (η_e), and the rf power delivered by the beam (P_e). As for the power from a dc supply, it is equal to the change of the potential energy of all electrons in the interaction space per unit time. The potential energy of the j-th macroparticle is given by the expression $W_j = q_0 U_a \ln(r_j / r_c) / [\ln(r_a / r_c)]$. Taking the derivative of this expression with respect to time, performing both averaging over a period of the rf-oscillations and summing up over all macroparticles, we arrive at the expression for the dc power:

$$P_0 = -q_0 \frac{U_a}{\ln(r_a / r_c)} \left\langle \sum_{j=1}^{K_p} \frac{\dot{r}_j}{r_j} \right\rangle . \qquad (33)$$

In terms of dimensionless coordinates used in Eqs. (27)-(31), this expression can be written as

$$P_0 = -\frac{q_0}{e_0} m_0 r_c^2 \Omega^3 S_0 , \qquad (34)$$

where $S_0 = \left\langle \sum_{j=1}^{K_p} A\dot{y}_j \right\rangle$ is a quantity describing the interaction of electrons with the dc field.

As it was noted before, the rf-power delivered by electrons to the rf-field is proportional to the I-value given by Eq. (25). This leads to the following expression for P_e:

$$P_e = -C_n R_e \langle I \rangle = -C_n^2 \frac{q_0}{G e_0} m_0 r_c^2 \Omega^3 S_1 . \qquad (35)$$

Thus, the electron efficiency can be calculated as

$$\eta_e = P_e / P_0 = C_n^2 \frac{S_1}{G S_0} . \qquad (36)$$

It is often necessary to know the anode current value, denoted by I_a. This value can be found from dc power as

$$I_a = \frac{P_0}{U_a} . \qquad (37)$$

A computer code has been developed to solve the above given system of equations and to study the physics of magnetron operation. The above mentioned peculiarities of SHM operation lead to the fact that the code requires more computer resources in comparison to codes used to simulate

the classical magnetrons. The dimensionless time step $\Delta\tau$ needed for the numerical solution of the equations of motion (29) and (30) is mainly determined by the rate of the variation of the rf-field amplitude which is experienced by the electrons. The spatial gradient of this amplitude is large due to the concentration of the field near the anode structure what requires small values of the time step compared to the cyclotron period. In the region near the anode, the $\Delta\tau$-value should be as low as 0.005. In other regions of interaction space, this value should be smaller than the characteristic transit time through a cell of the lattice which is used for the solution of Poisson's equation. In this case, the $\Delta\tau$-value is about 0.02.

Since Poisson's equation should be solved for the whole interaction space, a large number of sub-intervals M_φ along the azimuth coordinate is needed. In our simulations, this number is equal to 256, what corresponds to approximately 20 sub-intervals for one slow wave length. The number of sub-intervals M_y in radial direction is not so critical, a typical value being 48. The number of macroparticles within the interaction space K_p is related to the charge of a single macroparticle q_0. In order to have a smooth space-charge density distribution, it is desirable to have approximately 2-3 particles per one cell. Therefore, K_p should be larger than 30000. In our simulations, we used about 40000 macroparticles.

When simulating the classical magnetrons, only one spatial harmonic of the rf-field is usually taken into account. This is possible due to the fact that in classical magnetrons the amplitudes of the non-synchronous harmonics do not exceed the amplitude of the synchronous one, whereas in the case under consideration, the synchronous harmonic amplitude is small compared to the amplitude of the principal harmonic, so it is the latter one that should be taken into account.

VIII. Steady-State Oscillations

The mathematical model obtained allows the investigation of both transient and steady-state processes. If only the steady-state oscillation regimes are of interest then the computation procedure can be simplified, at first by neglecting the derivative in Eq. (27), i. e. $\dot{C}_n = 0$, and at second by neglecting the dependence of S_1 and S_2 on the phase. Strictly speaking, there are always some irregular variations of the amplitude. Since these variations occur at relatively low rate, it appeared, however, possible to assume $\dot{C}_n = 0$. As for the second assumption, it means that the "hot" frequency is constant in time. In this case, we have the following equations for the amplitude and phase instead of Eqs. (27) and (28):

$$S_1(C_n) = 1/Q_n, \tag{38}$$

$$\dot{\psi} = -\frac{\upsilon}{2} S_2(C_n). \tag{39}$$

Thus, in order to find values for the steady-state amplitude, the oscillatory characteristic $S_1(C_n)$ should be calculated. Provided the amplitude value is known, equation (39) gives the shift between the "hot" frequency and the "cold" one. It should be noted that even if the C_n-value is constant, there are still time variations of the oscillatory characteristics $S_1(C_n)$, $S_2(C_n)$. Therefore, these characteristics have been averaged over large time interval. An example of the calculation of the oscillatory characteristic $S_1(C_n)$ is given in Fig. 5. We have used the following set of magnetron parameters for the simulation: number of anode resonators of 16, anode radius of 2.25 mm, cathode radius of 1.3 mm, axial length of 6 mm, depth of the anode resonators of 1.385 mm, width of the anode resonators of 0.486 mm, anode voltage of 13.9 kV, dc magnetic field strength of 0.5875 T, operating frequency of 38.11 GHz, and the $\pi/2$ operating mode. In Fig. 5, two points (1 and 2), which are obtained as direct solution of the set of equations (27)-(31), have also been indicated. These points fit to the $S_1(C_n)$-curves fairly good what justifies the approach which has been based on the application of oscillatory characteristics for

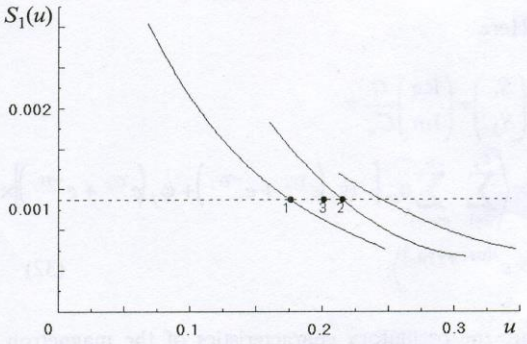

Fig. 5. *Oscillatory characteristic (solid curves). Points 1 and 2 indicate the calculated results obtained from the complete mathematical model. Point 3 indicates the result without taking the principal harmonic into account. The dashed line is given by the equation* $S_1 = 1/Q_n$ *for* $Q_n = 180$. *The intersection points of this line with the oscillatory characteristic define the amplitude values of steady-state oscillations*

the study of the steady-state regimes. In this figure, the result of the computer simulation has been indicated by point 3 for the case that the principal harmonic is not taken into account. A notable difference of this point location with respect to points 1 and 2 can be observed.

When the oscillatory characteristic $S_1(C_n)$ is known, stationary values of the field amplitude can be found as intersection points of the $S_1(C_n)$-curve with the horizontal line with ordinate equal to $1/Q_n$, as one can see in Fig. 5. It is found that the function $S_1(C_n)$ is multi-valued, and due to that there are several stationary states with different amplitude values for the same set of magnetron parameters. Thus, the magnetron is a multi-stable system. Multi-stable properties of a magnetron are well-known from the experiments [14], they could, however, not be explained till now in a reasonable way. Our simulation results indicate that such states may be related to the natural oscillations of the electron cloud. The peculiarity of the SHM consists in the fact that the rf-field is localized near anode and slightly affects the electron cloud oscillations near cathode, and, therefore, different stable states may be related to different modes of electron cloud oscillations. Figs. 6 and 7 show electron distributions for the above-mentioned stationary states, which correspond to

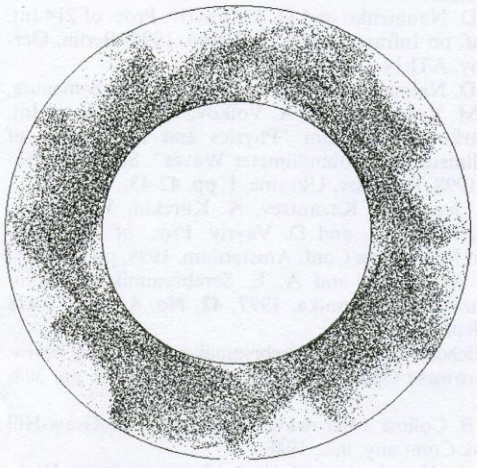

Fig. 6. *Space charge distribution for point 1 in Fig. 5*

points 1 and 2 in Fig. 5, respectively. It is obviously seen that although the rf-field distribution is the same for both cases, the electron distributions are essentially different. For example, it is possible to recognize four large scale characteristic periods in the azimuth direction in Fig. 6, whereas there are five such periods in Fig. 7. Simultaneously there is some spatial modulation which is related to the synchronous harmonic of the rf-field, which in this case has 12 periods. It is also obviously seen

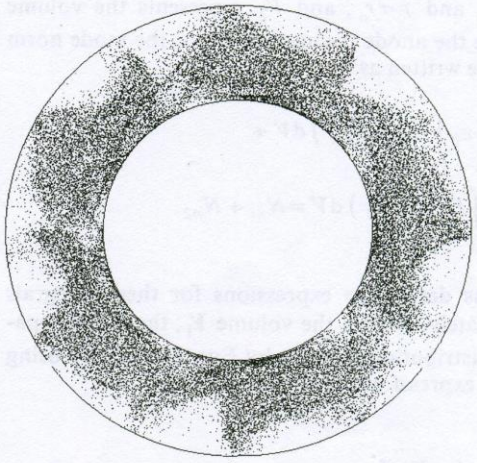

Fig. 7. *Space charge distribution for point 2 in Fig. 5*

from Figs. 6 and 7, that the interaction of cloud oscillations with different spatial periods leads to the formation of electron distributions, which do not show a periodical structure in an azimuth direction. Due to that, the SHM modelling requires the consideration of the whole interaction space rather than of an angle sector related with the rf-field period.

IX. Conclusions

In this paper, a self-consistent mathematical model of spatial-harmonic magnetron with secondary-emission cathode has been proposed. The model takes into account the space charge effects, secondary-emission, and nonlinear electron-wave interaction. It can be used for a detailed study of magnetron operation. It has been found that in order to describe adequately the operation of these magnetrons, the whole interaction space should be considered and the principal spatial harmonic should be taken into account together with the synchronous one. Multi-stable states of the SHM have been detected and their strong influence on the magnetron dynamics has been demonstrated.

Appendix

The mode norm N_n is defined by the following expression:

$$N_n = \varepsilon_0 \int_V \vec{E}_n(\vec{r})\vec{E}_n^*(\vec{r})dV .$$

It is written with respect to variables (r,φ,t), used in Eqs. (6), (7). The volume V represents the space which is occupied by rf field. It is convenient to represent this volume as a sum of two parts $V = V_1 + V_2$, where V_1 is a volume bounded by $r = r_c$ and $r = r_a$, and V_2 represents the volume inside the anode resonators. Thus, the mode norm can be written as:

$$N_n = \varepsilon_0 \int_{V_1} \vec{E}_n(\vec{r})\vec{E}_n^*(\vec{r})\,\mathrm{d}V + \\ + \varepsilon_0 \int_{V_2} \vec{E}_n(\vec{r})\vec{E}_n^*(\vec{r})\,\mathrm{d}V = N_{n1} + N_{n2}.$$

Let us derive the expressions for these integrals separately. Within the volume V_1, the rf-field spatial distribution is given by Eqs. (4), (5). By using these expressions, one obtains:

$$N_{n1} = \varepsilon_0 \int_0^L \mathrm{d}z \int_0^{2\pi} \mathrm{d}\varphi \int_{r_c}^{r_a} \left(E_{nr}(r,\varphi)E_{nr}^*(r,\varphi) + E_{n\varphi}(r,\varphi)E_{n\varphi}^*(r,\varphi)\right) r\,\mathrm{d}r = \\ = \varepsilon_0 L r_a^2 2\pi \left(\frac{2U_a M}{\pi d}\right)^2 \sum_{m=-\infty}^{\infty} \left(\frac{\sin\gamma\theta}{\gamma}\right)^2 \times \\ \times \int_0^{R_a} \frac{\left(R^{\gamma} - R^{-\gamma}\right)^2 + \left(R^{\gamma} + R^{-\gamma}\right)^2}{R\left(R_a^{\gamma} - R_a^{-\gamma}\right)^2}\,\mathrm{d}R = \\ = 2\pi\varepsilon_0 L r_a^2 \left(\frac{2U_a M}{\pi d}\right)^2 \sum_{m=-\infty}^{\infty} \left(\frac{\sin\gamma\theta}{\gamma}\right)^2 \frac{1}{\gamma} \frac{R_a^{\gamma} + R_a^{-\gamma}}{R_a^{\gamma} - R_a^{-\gamma}}.$$

As far as the width of the anode slots is essentially smaller than the anode radius, each of the resonators can be treated as a rectangular waveguide with shortened end. This waveguide has a length l and a cross-section (Ld). The rf-field distribution within the waveguide shows a single component E_n, which is given by

$$E_n = \frac{2U_a}{d} \frac{\sin(k(l-x))}{\sin kl},$$

where x is the coordinate along the waveguide with the origin at the anode surface. When writing this expression, the phase shift between the resonators is neglected since it has no influence on the norm value. The anode resonators are assumed to be equal, and thus their contributions to the mode norm are equal. The total contribution to the mode norm caused by the anode resonators is

$$N_{n2} = M\varepsilon_0 L \frac{4U_a^2}{d \sin^2 kl} \int_0^l \sin^2(k(l-x))\,\mathrm{d}x = \\ = \varepsilon_0 \frac{MLU_a^2}{kd \sin^2 kl}(2kl - \sin 2kl).$$

The values of N_{n1} and N_{n2} have the same order of magnitude. For example, for the set of parameters used here for simulations, we have $N_{n1}/N_{n2} \approx 2/3$. Therefore, no one of these values can be neglected.

Acknowledgement

The authors are indebted to Prof. Unger from Technical University Braunschweig, Germany, for stimulating and fruitful discussions and to the Deutsche Forschungsgemeinschaft for financial support. The work was also supported in part by EC under contract BIC15CT980509.

References

1. A. A. Slutzkin, S. Ya. Braude, I. D. Truten'. Radiotekhnika. 1946, **1**, No. 9, pp. 12-17 (in Russian).
2. I. M. Vigdorchik, V. D. Naumenko, V. P. Timofeev. Doklady Ukr. Akad. Nauk. 1975, **A**, No. 7, p. 633 (in Russian).
3. V. D. Naumenko and D. M. Vavriv. Proc. of 21st Int. Conf. on Infrared and mm-Waves. 1996, Berlin, Germany, ATh14.
4. V. D. Naumenko, K. Schünemann, V. Ye. Semenuta, D. M. Vavriv, and V. A. Volkov. Proc. of Third Int. Kharkov Symposium "Physics and Engineering of Millimeter and Submillimeter Waves". September 15-17, 1998, Kharkov, Ukraine, **1**, pp. 42-43.
5. M. Jenett, V. Kazantsev, A. Kurekin, V. Ryabov, K.Schünemann, and D. Vavriv. Proc. of 28th European Microwave Conf. Amsterdam. 1998, pp. 73-78.
6. D. M. Vavriv and A. E. Serebryannikov. Radiotekhnika i Elektronika. 1997, **42**, No. 4, pp. 472-478 (in Russian).
7. K. Schünemann, A. E. Serebryannikov, and D. M. Vavriv. Microwave Opt. Tech. Lett. 1998, **17**, No. 5, pp. 308-313.
8. G. B. Collins. Microwave Magnetrons. McGraw-Hill Book Company, inc., 1948.
9. L. A. Vainshtain and V. A. Solntsev. Super-High-Frequency Electronics. Moscow, Soviet Radio, 1973 (in Russian).
10. P. V. Romanov, A. S. Roshal'. Izv. VUZov. Radiofizika. 1971, **XIV**, No. 7, p. 1097 (in Russian).
11. C. K. Birdsall, A. B. Langdon. J. Comput. Phys. 1969, **3**, pp. 494-511.
12. I. M. Bronstain and B. S. Fraiman. Secondary Electron Emission. Moscow, Nauka Press, 1969 (in Russian).

13. J. Rodney and M. Vaughan. IEEE Trans. Electron Devices. 1989, **36**, No. 9, 1963.
14. V. Naumenko. Proceedings of the German-Ukrainian Seminar "Microwave Electronics: Theory, Devices, and Applications". Kharkov, Ukraine, 1996, pp.49-55.

монике по сравнению с классическими магнетронами. Описаны мультистабильные состояния магнетрона и предложен механизм их образования.

Математическая модель магнетрона на пространственной гармонике со вторично-эмиссионным катодом

К. Шунеманн, Д. М. Ваврив, С. В. Сосницкий

Предложена самосогласованная математическая модель магнетрона с вторично-эмиссионным катодом, работающего на пространственной гармонике. Модель предназначена для исследования как переходных, так и стационарных процессов. Описаны характерные особенности моделирования эффектов пространственного заряда, вторичной эмиссии, нелинейного взаимодействия электронов с волной. Представлены примеры результатов моделирования, иллюстрирующие отличия работы магнетронов на пространственной гар-

Математична модель магнетрона на просторовій гармоніці з вторинно-емісійним катодом

К. Шунеманн, Д. М. Ваврів, С. В. Сосницький

Запропоновано самоузгоджену математичну модель магнетрона з вторинно-емісійним катодом, працюючого на просторовій гармоніці. Модель призначена для дослідження як перехідних, так і стаціонарних процесів. Описано характерні особливості моделювання ефектів просторового заряду, вторинної емісії, нелінійної взаємодії електронів з хвилею. Надано зразки результатів моделювання, які ілюструють особливості роботи магнетронів на просторовій гармоніці порівняно зі звичайними. Описано мультистабільні стани магнетрона та запропоновано механізм їх утворення.